Proceeding of the 13th National Mechanical Engineering Conference
2-3 December 1999, Royal Cliff Beach Resort Hotel, South Pattaya, Cholburi

Ground Effect on The Aerodynamic Characteristics of A Cylinder in Subcritical Flow

Piyasak Damronglerd, Pitipong Yenjit, Kobchai Wasuthalainun, Paradon Khemakanok
Alongkorn Pimpin and Asi Bunyajitradulya

Fluid Mechanics Research Laboratory, Department of Mechanical Engineering,
Faculty of Engineering, Chulalongkorn University,
Bangkok 10330, Thailand
Tel. 218-6645, 218-6647; Fax. 252-2889; E-mail basi@chula.ac.th

Abstract

Ground effect on pressure distribution and aerodynamic force coefficients of a cylinder in subcritical flow is investigated. The flow has a Reynolds number based on the cylinder diameter D of 1.6×10^4 and has a relative wall boundary layer 95% thickness δ_w / D and a relative displacement thickness δ_1 / D measured at 4 diameters upstream of the cylinder of 1 and 0.26, respectively. The gap width d between the cylinder and the wall is varied for eight values corresponding to d / δ_1 of 0.9, 1.8, 2.7, 3.6, 4.5, 5.4, 7.2, and ∞.

The results show that the observed changes in pressure distribution and force coefficients can be roughly divided into three regimes: $d / \delta_w > 1$, $d / \delta_w < 1$ and $d / \delta_1 > 1$, and $d / \delta_1 <\sim 1$. Different characteristic parameters behave differently in these regimes. Generally and most importantly, though, as the gap width decreases, a reduction in maximum pressure coefficient, a delay in the angular position of local maximum pressure just ahead of the wake region – an approximate point of separation, and a reduction in the extent of the wake region are observed. The latter two are consequences of a triggered and early transition from laminar to turbulent of the boundary layer on the near wall surface of the cylinder. The triggering agent for this early transition is attributed to turbulence in the wall boundary layer, which acts in much the same way as freestream turbulence. For the aerodynamic force coefficients, it is found that the gap width has a drastic impact when d / δ_1 is comparable to or less than one, elsewhere it has little or no effect. In the former, a reduction in drag and an increase in lift coefficients are observed.

The paper describes in details the effects of gap width on characteristic pressures as well as on characteristic angular positions associated with the pressure distribution $C_p(\theta)$

1. Introduction

Aerodynamics (or hydrodynamics) is a subject of great importance for not only in the obvious area of vehicle design (automobiles, airplanes, ships, trains, etc.), but it often plays significant role in other areas such as dynamics, structural dynamics and design, noise and vibration, etc. This is mainly because of the aero/hydro-dynamic force exerted on a submerged body. One aspect of the aerodynamics of a submerged body that often comes up in many applications is the *ground* or *wall effect*. In short, the presence of ground or wall in the proximity of a body changes the flow field characteristics around that body through inviscid and/or viscous phenomena, thus causing changes in the nature and the magnitude of aerodynamic forces on the body.

In this study, ground effect on the aerodynamic characteristics of a cylinder in crossflow which, otherwise, is in the subcritical flow regime is investigated. Specifically, for various gap widths pressure distributions on the circumference are measured and the lift and drag coefficients are determined. From the results, the ground effects on strategic aerodynamic characteristics of a cylinder are examined.

2. Dimensional analysis

To study the ground effect on the aerodynamic characteristics of a cylinder in crossflow, we pose the following dimensional analysis problem: Given the flow configuration, the pressure distribution on the circumference of a circular cylinder is desired. Therefore, we choose the list of nine relevant parameters, independent or not, in this problem as freestream velocity u_∞, density ρ; viscosity μ; diameter of a cylinder D, gap size measured between the cylinder surface and the wall d, the boundary layer thickness on the wall δ_w, the boundary layer thickness on the cylinder δ_c, the angle θ, and the corresponding local pressure coefficient C_p, defined as

$$C_p = \frac{p - p_\infty}{\frac{1}{2}\rho u_\infty^2}, \qquad (1)$$

where p is a local static pressure at θ and p_∞ is the freestream static pressure. Figure 1 illustrates the flow configuration as well as the coordinates system adopted. Note that for the most part in this paper we shall use the angular coordinates $-180° < \theta < 180°$ although at times we shall switch to $0° < \theta < 360°$ for convenience; no confusion should or could be arised by this, however.

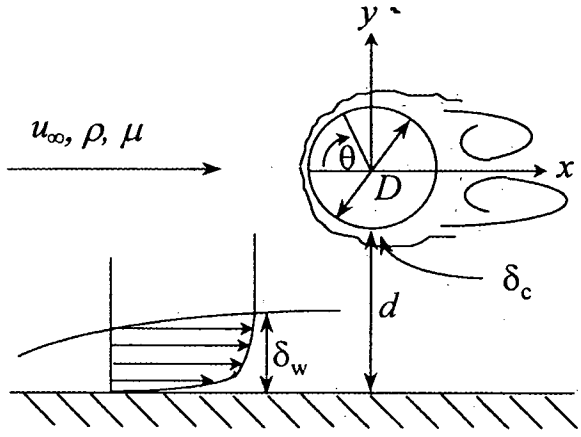

Fig. 1. Schematic sketch of flow past a circular cylinder near wall. The relevant parameters are indicated.

Using dimensional analysis, one obtains six dimensionless parameters which can be written in a functional form as

$$C_p = f(\theta; \mathrm{Re}_D, \delta_w / d, \delta_w / D, \delta_c / D), \quad (2)$$

where $\mathrm{Re}_D = \rho u_\infty D / \mu$ is the Reynolds number based on the cylinder diameter.

For the case of a cylinder in freestream, or without ground effect, δ_c, say at the location $\theta = -90°$, is dependent on Re_D for a given surface roughness. Therefore, it is conceivable that in the presence of a wall and for a given surface roughness δ_c is dependent on Re_D and δ_w / d; hence, we drop δ_c / D from Eq. 2 and obtain

$$C_p = f(\theta; \mathrm{Re}_D, \delta_w / d, \delta_w / D) \quad (3)$$

By replacing δ_w / D with d/D, Eq. 3 can also be rewritten as

$$C_p = f'(\theta; \mathrm{Re}_D, \delta_w / d, d / D). \quad (4)$$

It is insightful from the point of view of an experiment to discuss the difference between the functional forms of C_p in Eqs. 3 and 4. Specifically, the functional form of C_p employed dictates the setting up of the experiment, and vice versa. For example, if the effect of the width of the gap d / δ_w on C_p is desired and Eq. 3 is employed, Re_D and δ_w / D need to be fixed. Experimentally, this can be done quite simply by using a cylinder of diameter D, running the wind tunnel at constant speed u_∞, and fixing the streamwise location of the cylinder while varying the gap d. By fixing the streamwise location of the cylinder as d is varied, δ_w / D is fixed. (This is provided that the reference point for measuring δ_w is far upstream enough so that δ_w is not affected by the upstream influence of the flow ahead of the cylinder.) On the other hand, if Eq. 4 is employed, the experimental setup becomes more complicated because of the change in d/D as d is varied. In this setup, one needs to change the cylinder to a different size every time d is varied in order to keep d/D constant.

Therefore, in this study the experiment is designed around the functional form as represented by Eq. 3.

3. Experimental setup

The experiment was conducted in the Fluid Mechanics Research Laboratory (FMRL), Department of Mechanical Engineering, Faculty of Engineering, Chulalongkorn University. The wind tunnel used is a modification of the existing suction type tunnel shown schematically in Fig. 2. After room air is drawn through a bell-mouth inlet, it passes through a settling chamber which consists of, from upstream to downstream, mesh-20 screen; a honeycomb made from plastic drinking straws (6 mm dia., 15 cm long) sandwiched between two mesh-20 screens, a series of four mesh-20 screens and a mesh-30 screen. All screens are uniformly spaced at 100 mm apart. Then, air is drawn into a test section which has a cross section at the inlet of 12x12 in^2 and a length of 200 cm. All four walls of the test section are made of acrylic plate of 10 mm in thickness. Owing to the anticipated blockage effects of the growing boundary layer as well as of the cylinder itself, the test section is equipped with a flexible upper wall. In short, the upper wall is a cantilever supported by a flange at the test section inlet and two adjustable screw hangers located at 125 cm and 200 cm from the inlet. The shape of the upper wall can then be adjusted by means of these two screws. At the end of the test section is a reducer of 130 cm long. The reducer connects the test section, which at this location may have a height more than 12 in, to a 12x12 in^2 inlet of an adapter-diffuser of another 100 cm long. At the top portion of an inlet of the reducer is a gap between the adjustable upper wall and the fixed height reducer, hence some room air is drawn through this gap during operation. At the end of the adapter-diffuser is a butterfly valve leading to a 5.5-kw axial flow fan. The wind speed in the test section can then be adjusted by means of this butterfly valve. The air drawn into the tunnel is discharged back to atmosphere at the end of the tunnel.

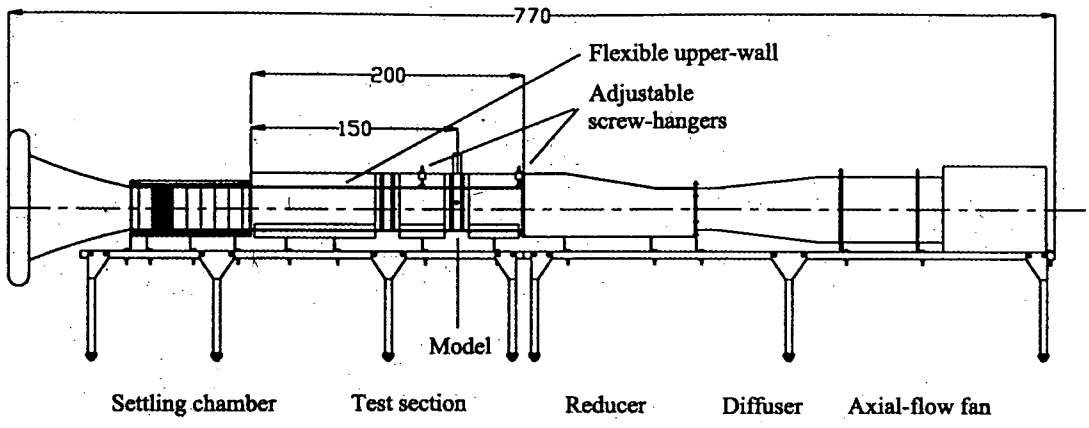

Fig. 2. Schematic diagram of the wind tunnel.

The test cylinder is located at 150 cm downstream of the test section inlet. It is an acrylic pipe 25 mm in outer diameter. To be able to adjust the gap width d, the cylinder is mounted on a sliding side-plate assembly which can be slided vertically along the side wall and whose inner surface lies flushed on the same plane as that of the side wall. When the desired gap width is set, the assembly is press fitted to the side wall on both sides, left and right, by means of screws. Figure 3 illustrates the sliding side-plate assembly.

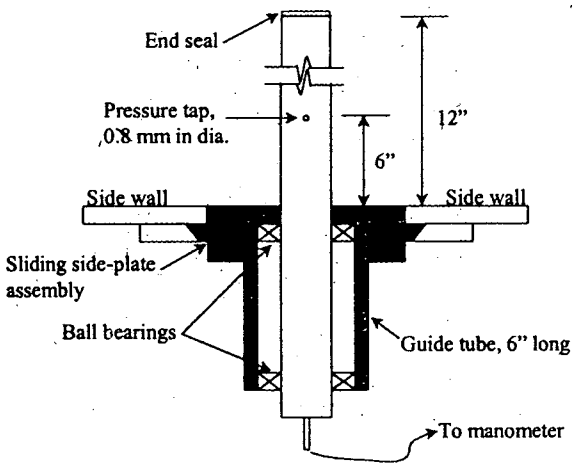

Fig. 3. Schematic of the sliding side-plate assembly (top view).

On the test cylinder, at the mid-span location corresponding to the center of the tunnel, is a static pressure tap of 0.8 mm in diameter. The test cylinder is supported by two ball bearings, located approximately 6 inches apart, in order that the relative angular position of the pressure tap with respect to the direction of the freestream velocity can be adjusted to the desired value of θ, enabling the measurements of static pressure at various θ's by means of only one pressure tap. In addition, the separation of 6 inches between the two ball bearings helps minimizing the pitch angle of the cylinder (measured relative to its own axis) owing to any backlash.

Diagnostic tools employed were a pitot probe and static pressure taps. The pitot probe is a laboratory-built one with inner diameter of 0.8 mm and outer diameter of 1.2 mm, the details of which can be found in the companion paper by Sakulyanontvittaya et al. (1999). It was used for the measurements of freestream velocity as well as the incoming boundary layer profile. The static pressure taps were of two sets: one just described was for the measurement of static pressure distribution on the circumference of the cylinder and the other was a set of static pressure taps along the tunnel's upper and lower walls. The taps along both walls were uniformly spaced at 10 cm apart. These taps were used to monitor the static pressure distribution in the tunnel so that the flexible upper wall could be adjusted to the desired pressure distribution. These experiments were conducted at constant pressure condition.

An inclined manometer with a resolution of 0.2 mm water was used for all pressure measurements. In addition, all the measurements of pressures were done with respect to the reference static pressure tap (p_{ref}) located on the upper wall at 4 diameters upstream of the cylinder.

The boundary layer on the tunnel floor was used as a test boundary layer. Therefore, the gap width d was measured from this wall. The measurement of the incoming boundary layer profile was done at the reference location, 4 diameters upstream of the cylinder. The spatial resolution of the measurement was 1 mm, i.e., the pitot probe was traversed at 1 mm step away from the wall.

The measurements of the static pressure distribution on the circumference of the cylinder were done at 5° step, i.e., the cylinder was rotated at 5° step.

The experiments were conducted at the freestream velocity of 10 m/s, corresponding to Re_D in a subcritical flow regime of 1.6×10^4. At this speed, the incoming boundary layer on the tunnel floor, measured at the

reference location, had a 95% thickness, δ_w, and a displacement thickness, δ_1, of 25 mm and 6.5 mm respectively, giving $\delta_w / D = 1$ and $\delta_1 / D = 0.26$. The gap d was varied for 8 values: 5.5, 11.5, 17.5, 23.5, 29.5, 35.5, 47.5, and 150 which are corresponding to d/δ_1 of 0.9, 1.8, 2.7, 3.6, 4.5, 5.4, 7.2, and ∞ (no wall or freestream condition).

4. Results

4.1. Boundary layer profile and boundary layer thickness

In the determination of the boundary layer thickness, the boundary layer profile was measured with a laboratory-built pitot probe and a static pressure tap at the reference location, 4 diameters upstream of the test cylinder. The measured profile was then used for the calculation of the 95% and the displacement thickness without any priori correction for the effect of the size of the probe. Figure 4a shows the measurement result on a Clauser's plot, u/u_∞ VS $\mathrm{Re}_y = u_\infty y/\nu$ on a semi-log plot, Clauser (1954). In the figure are also shown for comparison the plots for boundary layers with skin friction coefficients C_f of 0.0030, 0.0033, and 0.0036. From the plot, the skin friction coefficient of the boundary layer was then determined to be between 0.0033 and 0.0036 with the best fit in the log region at 0.0035. The result was then used for the calculation of the profile according to Cole's law of the wake (Coles, 1956),

$$u^+ = \frac{1}{\kappa}\ln y^+ + B + \frac{\Pi}{\kappa} W\left(\frac{y}{\delta}\right) \tag{5}$$

or

$$\frac{u}{u_\infty} = \left[\frac{1}{\kappa}\sqrt{\frac{C_f}{2}}\ln\left(\sqrt{\frac{C_f}{2}}\,\mathrm{Re}_y\right) + B\sqrt{\frac{C_f}{2}}\right] + A\sin^2\left(\frac{\pi}{2}\frac{\mathrm{Re}_y}{\mathrm{Re}_\delta}\right)\sqrt{\frac{C_f}{2}} \tag{6}$$

where $u^+ = u/u_\tau$, $u_\tau = \sqrt{\tau/\rho}$, $y^+ = y u_\tau/\nu$, $\mathrm{Re}_\delta = u_\infty \delta/\nu$, $\Pi = \kappa A/2$, $W(y/\delta) = 2\sin^2(\frac{\pi}{2}\frac{y}{\delta})$, $\kappa = 0.41$, B=5.0, A=2.35. In this case the best fit is at $C_f = 0.0033$, and the result is shown in the same figure. Figure 4b shows the same data on a linear plot. The measured data fitted Cole's law fairly well except in the near wall region, approximately within 4 mm from the wall. This is to be expected owing to the size of the probe. From the measured data, the 95% thickness δ and the displacement thickness δ_1 were determined to be 25 and 6.5 mm respectively.

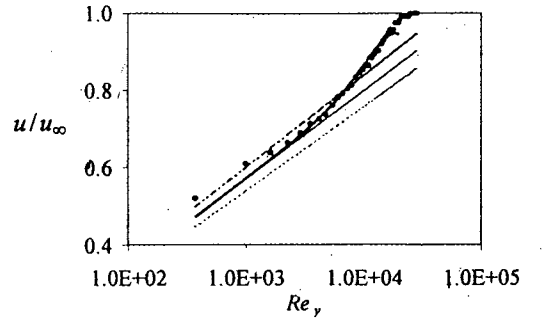

Experimental data $C_f = 0.0030$ — $C_f = 0.0033$
$C_f = 0.0036$ — Coles's Law

(a)

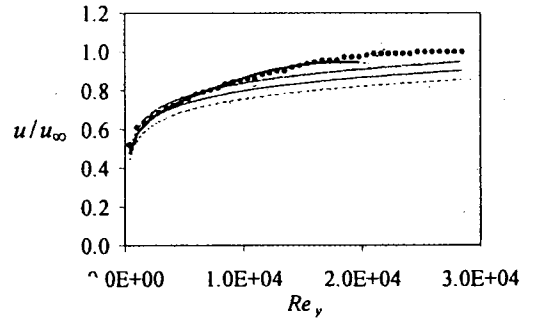

Experimental data $C_f = 0.0030$ — $C_f = 0.0033$
$C_f = 0.0036$ — Coles's Law

(b)

Fig. 4. Boundary layer profile at the reference location: (a) on semi-log plot, (b) on linear plot.

4.2 Pressure distributions and aerodynamics coefficients

All the results related to the pressure distribution and the aerodynamic characteristics are summarized in Table 1 (see back) together with the estimates of experimental uncertainty. The nomenclatures are given below. In processing the data for the distributions of the static pressure, $C_p(\theta)$, we correct for an error in angular position owing to misalignment by taking the angular position of the point of maximum $p - p_{ref}$ in case $d/\delta_1 = \infty$ as an offset. The offset value is then subtracted from all other data points. This maximum $p - p_{ref}$ value is also taken as the dynamic pressure of the fresstream, Eq. 1. Thus, for the determination of C_p for all other data points, the corresponding value of $p - p_{ref}$ are normalized by this maximum value. As a result, the uncertainties in the measured angular position θ and in the calculated pressure coefficient C_p are estimated to be within $\pm$ 2.5° and $\pm$ 0.03 respectively. Note that because of the finite size of the pressure tap (0.8 mm), the reading of the pressures is approximately an average value over $\pm$ 1.8°.

Figures 5a (see back) shows the results for static pressure distributions on the circumference of the cylinder for cases $d/\delta_w < 1$: $d/\delta_1 = 0.9$, 1.8, and 2.7; and Fig. 5b, for cases $d/\delta_w > 1$: $d/\delta_1 = 4.5$, 5.4, and 7.2. Cases $d/\delta_1 = 3.6$ ($d/\delta_w = 0.94$) and ∞ are repeated in both figures for comparison. Note that, for cases in Fig. 5a part of the lower surface of the cylinder is submerged in the wall turbulent boundary layer ($d/\delta_w < 1$), while that for cases in Fig. 5b the cylinder is clear from the boundary layer ($d/\delta_w > 1$).

Also shown in the figures is the corresponding static pressure distribution according to the inviscid theory,

$$C_p(\theta) = 1 - 4\sin^2\theta . \qquad (7)$$

As is obvious from the results, all cases have common characteristics as depicted in Fig. 6; therefore, for convenience, we shall use the following notations:

- $C_{p\max}$ the maximum value of C_p;
- $C_{p\min}$ the local minimum value of C_p ahead of the wake region;
- C_{pw} the average value of C_p in the wake region;
- $\gamma_{\min}$ the angular position of $C_{p\min}$;
- $\gamma_{\max}$ the angular position of the local maximum just ahead of the wake region;
- γ_o the angular position of the zero-crossing;
- $\Delta\gamma_{\min}$ the angular distance between $\gamma_{\min 1}$ and $\gamma_{\min 2}$ measured across the leeward surface;
- $\Delta\gamma_{\max}$ the angular distance between $\gamma_{\max 1}$ and $\gamma_{\max 2}$ measured across the leeward surface;

subscripts 1 and 2 refer to the upper and the lower surface respectively.

In addition, we shall use the notion of quadrant to indicate the angular position: Q_1: $0° < \theta < 90°$; Q_2: $90° < \theta < 180°$; Q_3: $-180° < \theta < -90°$; Q_4: $-90° < \theta < 0°$.

General characteristics

For all cases tested, i.e., $d/\delta_1 = 0.9$ to ∞, the results show no drastic change in the general characteristics of the pressure distribution, $C_p(\theta)$. That is, there is a local maximum of pressure at or near the nose (θ = 0°) followed by a descending to zero and to a local minimum near each pole (north-south) and then by a local maximum that levels off to a flat region on the leeward surface of the cylinder. From the case of a cylinder in freestream, it can be inferred that separations on both upper and lower surfaces occur approximately at $\theta = \pm 83°$. (In general, separation occurs approximately at the location of $\gamma_{\max}$, see Table 1.) This implies that the boundary layers on the cylinder surfaces still remain laminar at the points of separations. Hence, the flow is subcritical. In addition, for this freestream case, the well-known characteristics of the distribution approaching that predicted by inviscid theory near the nose is observed.

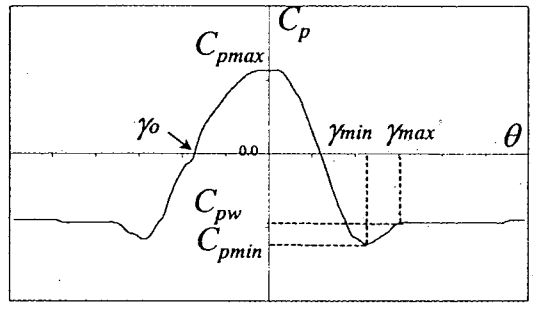

Fig. 6. Notations for characteristic points on C_p VS θ.

On the other hand, an increase in the degree of asymmetry of $C_p(\theta)$ as d/δ_1 decreases is obvious. For cases of high d/δ_1, specifically for cases in Fig. 5b in which $d/\delta_w > 1$, the pressure distribution is symmetric and approaches that of the freestream case with an almost exact replica from the nose upto approximately the point of minimum pressure ($-|\gamma_{\min 2}| < \theta < \gamma_{\min 1}$), after which point some deviation is observed on the leeward surface. The deviation is nonetheless minor that a fraction of it can be contributed to experimental uncertainty. As d/δ_w decreases below 1 but d/δ_1 still above 1 (Fig. 5a), the most obvious change is the reduction in $C_{p\max}$. Nonetheless, the pressure distribution is still very much symmetric except for case $d/\delta_1 = 1.8$ in which some deviation from symmetry is observed starting approximately 10° after the point of zero-crossing on the lower surface (γ_{o2}). When d/δ_1 is comparable to 1 as in case $d/\delta_1 = 0.9$, asymmetry in $C_p(\theta)$ is pronounced, starting practically right at the nose.

Another related observation is the curvature of $C_p(\theta)$ at the nose. The change in characteristics is similar to the asymmetry discussed above. That is, it is observed to depend on three regimes: $1 < d/\delta_w$, $d/\delta_w < 1$ and $1 < d/\delta_1$, and $d/\delta_1 < \sim 1$. Note that the change may not be abrupt, nonetheless it is noticeable. For cases with $1 < d/\delta_w$, practically no change is observed. For cases with $d/\delta_w < 1$ and $1 < d/\delta_1$, slight change can be observed for which in this case is the reduction in curvature. And, for case with $d/\delta_1 < \sim 1$, a significant or drastic change is observed. In the latter case, for case $d/\delta_1 = 0.9$ an almost flat region spanning approximately 15° from θ = -7.5° to +7.5° is observed.

Another drastic and obvious change can be seen in the level of C_p in the wake region, or C_{pw}. Here we define the wake region as the region that lies between

γ_{max1} and γ_{max2} measured across the leeward surface, i.e., $\gamma_{max1}<\theta<180°$ U $-180°<\theta<\gamma_{max2}$, because the points of separation that are the origins of wake on the upper and lower surfaces can be approximated by the corresponding locations of γ_{max1} and γ_{max2}. For this, no significant change in C_{pw} relative to the value of the freestream case is observed for cases $1<d/\delta_w$. For cases in which $d/\delta_w<1$ and $1<d/\delta_1$, however, a significant reduction in C_{pw} is observed. In contrast, as d/δ_1 decreases further until $d/\delta_1<1$ as in the case $d/\delta_1=$ 0.9, a drastic increase in C_{pw} is observed.

We shall now present each and additional characteristics in details.

C_{pmax}, C_{pmin}, C_{pw}

Figure 7 depicts the change in characteristic C_p's as the width of the gap change. Also shown in the figure is the uncertainty in measurements which is estimated to be $\pm$ 0.03 for all C_p's.

As the results show, C_{pmax} starts decreasing as d/δ_w decreases below 1. This implies that the "mean" streamline that leads to the point of C_{pmax} moves closer to the wall as d/δ_w decreases. We shall discuss this in more details in the next section.

On the other hand, C_{pmin1} and C_{pmin2} change by practically equal amount as d/δ_1 decreases – down to the case d/δ_1=0.9, making the change – at least in magnitude – symmetric with respect to the upper and the lower surfaces. In other words, C_{pmin1} and C_{pmin2} are always equal even when the gap is reduced to $0.9\delta_1$. As we shall soon see, however, that this is not the case for the locations of C_{pmin1} and C_{pmin2}.

As the gap decreases below δ_w but still above δ_1, slight decrease in C_{pmin} (1 and 2) is observed. As the gap decreases further below δ_1, however, a drastic increase by almost 40% is observed. This change in characteristics is echoed with a slight decrease followed by the corresponding drastic increase by pressure distribution in the wake region behind the cylinder, indicated by C_{pw}.

Note that as a fluid particle moves downstream, from the nose, along the circumference of a cylinder, it experiences a decrease in pressure upto the point of minimum pressure, γ_{min}. After that, it regains pressure for a short interval upto approximately the point of local maximum pressure γ_{max}, before the boundary layer separates. The pressure recovery after the point of minimum pressure is then given by $C_{plocal\ max}-C_{pmin}$, where $C_{plocal\ max}$ is the local maximum which is approximated by C_{pw}. A closer look at the pressure recoveries on both upper and lower surfaces is given in Fig. 8, together with the uncertainty estimates. In this case the uncertainty estimates are given as $\pm$ 0.04 although for the cases with $d/\delta_w>1$, they are more likely less. From the figure, despite the uncertainty the pressure recoveries are observed to generally decrease as d/δ_1 decreases.

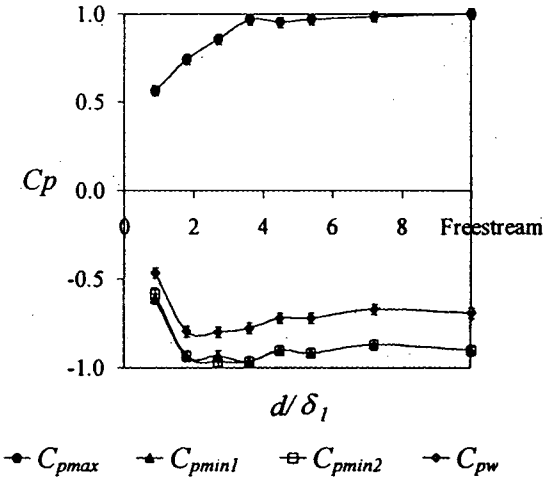

Fig. 7. Effects of the gap width on characteristic pressure coefficients.

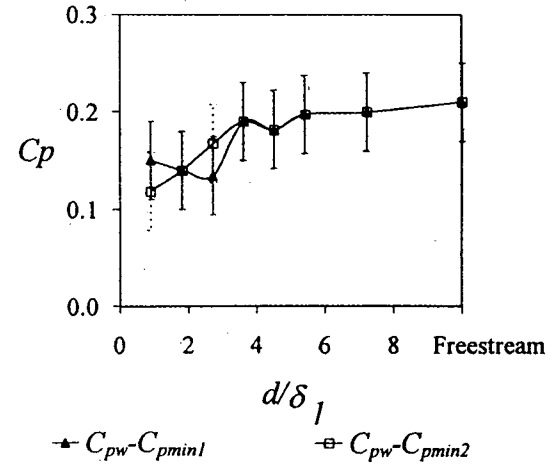

Fig. 8. Effects of gap width on pressure recoveries.

γ_{max}, γ_{min}, γ_o

Better understanding of the flow comes not from the characteristic pressure coefficients but from the characteristic positions. Figure 9 (see back) shows the results for various characteristic angles together with the estimates of experimental uncertainty.

The angular position for a local minimum pressure is designated by γ_{min}. From the figure, it can be seen that

the gap width has relatively little or no effect on $\gamma_{\min 1}$. On the other hand, it gradually has strong effect on $\gamma_{\min 2}$, starting right from $d/\delta_w \sim 1$, and causing a delay in reaching a local minimum pressure. For case $d/\delta_1 = 0.9$, the delay is approximately 20° relative to the case of freestream. Thus, it is seen that the reduction in gap width below δ_w causes asymmetric change in the locations of local minimum pressures on the upper and the lower surfaces. This is clearly in contrast to its effect on $C_{p\min}$ in two aspects as discussed above. Specifically and firstly, unlike its effect on $\gamma_{\min}$, the reduction in gap width causes a symmetric and equal change in $C_{p\min 1}$ and $C_{p\min 2}$. And, secondly, it starts to have significant and, in fact, sudden effect on $C_{p\min}$ only when $d <\sim \delta_1$.

The state of affairs is revealed when the positions of local maximum pressure, $\gamma_{\max}$, are examined. But before the results are presented, some words regarding the determination of $\gamma_{\max}$ are in order. Unlike the local minimum, the local maximum, if it exists, is relatively difficult to be determined owing to the gradual leveling off of C_p towards C_{pw}, together with the relatively low resolution of the experimental setup. Therefore, as mentioned earlier we take C_{pw} as the representative value for this local maximum. $\gamma_{\max}$ is then defined as the first angular position approached, from the point of the corresponding local minimum, at which the corresponding C_p lies within the experimental uncertainty of C_{pw}, i.e., $C_p \geq C_{pw}$-0.03.

As mentioned earlier, the position of $\gamma_{\max}$ corresponds approximately to the point of boundary layer separation. For subcritical flow, in which the separated boundary layer is laminar, separation occurs at $\theta \sim 82°$; and for supercritical flow, in which the separated boundary layer is turbulent, $\theta \sim 120°$ (White, 1994). The results, shown in Fig. 9 and Table 1, indicates that for the freestream case $\gamma_{\max 1} \sim |\gamma_{\max 2}| \sim 83°$; hence, the separated boundary layer is laminar and the flow is subcritical on both upper and lower surfaces. As the gap width d decreases, $\gamma_{\max 1}$ and $|\gamma_{\max 2}|$ increase approximately equally - making a symmetric change in the locations of local maxima – until the gap width is reduced to $d/\delta_1 = 2.7$, at which point the points of local maxima are delayed by an equal amount of approximately 10°. As d decreases further, however, $\gamma_{\max 1}$ remains approximately constant at 88°-93° while $|\gamma_{\max 2}|$ continues to increase to 103° for $d/\delta_1 = 0.9$. Initially, the delay in $|\gamma_{\max 2}|$ is relatively slow, by 10° from $d/\delta_1 = \infty$ to 2.7. From $d/\delta_1 = 2.7$ to 0.9, however, the delay is accelerated, by an additional amount of 10°.

The delay in $|\gamma_{\max 2}|$ from 83° in the freestream case to 103° in the case $d/\delta_1 = 0.9$ suggests the corresponding delay in boundary layer separation. This suggests that the boundary layer on the lower surface for cases of low d/δ_1, particularly case $d/\delta_1 = 0.9$, is *not* laminar *but* turbulent when it separates. This implies that early transition from laminar to turbulent must have been induced and, as a consequence, results in the ability of the boundary layer to remain attached for additional 20° (from 83° to 103°). Realizing that for cases with low d/δ_1, particularly cases with $d/\delta_w < 1$, part of the lower surface is submerged in the turbulent boundary layer (for a fraction of time approximately equal to the local intermittency factor at the edge of the boundary layer), one is not surprised of the source of trigger for early transition. That is, turbulence in the wall boundary layer acts as the triggering agent for early transition for the boundary layer on the cylinder lower surface – in much the same way as the effect of freestream turbulence on transition.

What is rather intriguing, however, is the fact that the characteristics of $\gamma_{\max 1}$ is very similar to that of $\gamma_{\max 2}$ in the range of $2.7 \leq d/\delta_1 < \infty$ despite the fact that the upper surface is pointed away from the wall. In addition, given this, it is also intriguing from the point of view of $\gamma_{\max}$ that the effect of the wall can be felt as far as $d/\delta_1 = 7.2$ or $d/\delta_w = 1.9$ ($\gamma_{\max 1}$=83° and 88° for $d/\delta_1 = \infty$ and 7.2, respectively.)

Figure 9 also shows the points of zero-crossing, γ_o. It is seen that, except for the lower surface of case $d/\delta_1 = 0.9$, the gap width d has little effect on the zero-crossing either on the upper surface or on the lower surface. For the lower surface of case $d/\delta_1 = 0.9$, γ_{o2} changes as much as 14° Another characteristics shown in Fig. 9 is the angular interval for pressure recovery, indicated by $(\gamma_{\max 1} - \gamma_{\min 1})$ and $|\gamma_{\max 2} - \gamma_{\min 2}|$. Fluctuations on both surfaces are observed as the wall is approached, though the general trend seems to be increasing.

Figure 10 (see back) is a replot of Fig. 5 in the angular coordinate $0° < \theta < 360°$ so that the extent of the wake region, indicated by $\Delta\gamma_{\max} = \gamma_{\max 2} - \gamma_{\max 1}$, can be examined more closely, and the results are summarized in Fig. 11 below. The results indicate that for cases with $d/\delta_w > 1$, the extent of the wake region is uniformly affected by the gap width, an approximate reduction of 12°. As d/δ_w decreases below 1, however, the extent of the wake region on the lower surface progressively starts to contract, causing a total reduction of the wake region as much as 30° for case $d/\delta_1 = 0.9$. Also shown in the figure is $\Delta\gamma_{\min}$. The reduction in $\Delta\gamma_{\min}$ occurs only when $d/\delta_w < 1$.

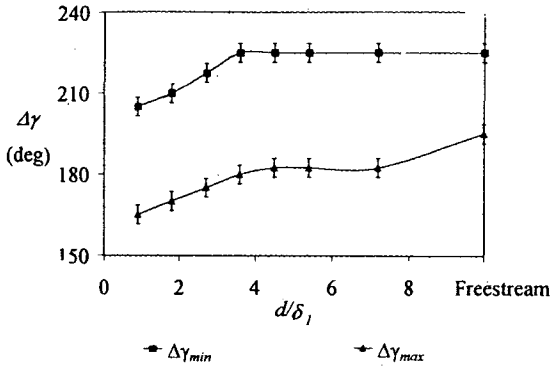

Fig. 11. Effects of gap width on the extent of the wake region, $\Delta\gamma_{max}$, and $\Delta\gamma_{min}$.

C_L and C_D

The effects of gap width on the lift and drag coefficients as well as on the lift-per-drag ratio are shown in Fig. 12. The results show relatively no effect on C_D for cases with $d/\delta_w>1$. As d/δ_w decreases below one, however, C_D first increases slightly but then decreases drastically as d/δ_1 falls below 1. The drastic decrease in C_D is owing to a reduction in $C_{p\max}$ as well as a significant increase in C_{pw}. On the other hand, a drastic increase in C_L is observed for case $d/\delta_1<1$, elsewhere C_L is not affected by gap width. This is undoubtedly a result of an asymmetry in $C_p(\theta)$ which is, in turn, is a result of early boundary layer transition and delayed separation. Consequently, the lift-per-drag ratio remains zero for all cases except for case $d/\delta_1<1$ in which a jump to 0.17 is observed.

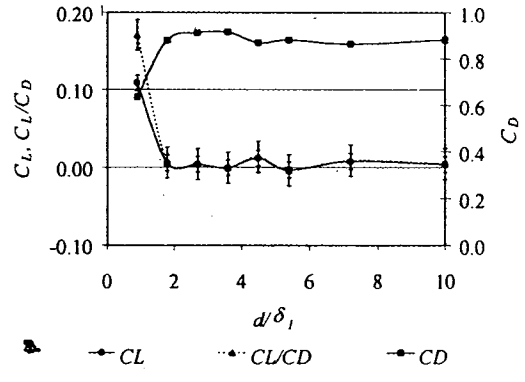

Fig. 12. Effects of gap width on lift and drag coefficients.

5. Discussion

The reduction in $C_{p\max}$ with d/δ_w is worth examining in more details. The fact that $C_{p\max}$ decreases as d/δ_w decreases below one implies that the "mean" streamline that leads to the point of $C_{p\max}$ comes from within the boundary layer and that it moves closer to the wall as d/δ_w decreases. In addition, since the angular position of $C_{p\max}$ almost remains unchanged, i.e., remains at the nose (Fig. 5a), for cases d/δ_1=1.8 and 2.7 and possibly changes but relatively little for case d/δ_1=0.9, this further implies large deflection of the leading streamline away from the wall as it approaches the cylinder.

In addition, a reduction in $C_{p\max}$ can be used to locate the approximate position of the leading streamline. For example, for case d/δ_1 = 0.9, the reduction of $C_{p\max}$ to approximately 0.5 times of the freestream case gives a rough estimate of the mean velocity of the leading streamline to be $u_\infty/\sqrt{2}$. Hence, this gives (Fig. 4) the estimated location of the leading streamline to be at 5-6 mm from the wall, an order of the gap d. Similar arguments can be made for cases d/δ_1 = 1.8 and 2.7, and the estimated location of the leading streamline is found to be in the order of the gap d from the wall

Another related point that is worth noting is the fact that the curvature of $C_p(\theta)$ at the nose decreases as d/δ_w decreases below one. In other words, the pressure distribution in the neighbors of the nose becomes more uniform as d/δ_w decreases below one. This is likely owing to the mixing nature of turbulence that tends to make flow properties become more uniform.

6. Conclusions

Ground effects on pressure distribution and aerodynamic coefficients of a cylinder in subcritical flow were investigated. The results showed that, as the gap width decreased such that the near wall surface of the cylinder was in the vicinity of the wall turbulent boundary layer, early transition from laminar to turbulent of the boundary layer on that surface was promoted by the trigger from turbulence that was originated from the wall boundary layer – in as much the same way as the effect of freestream turbulence on transition. This caused a delay in separation and, in effect, caused a change from laminar boundary layer separation to turbulent boundary layer separation, or from subcritical flow to supercritical flow. As a result, the extent of the wake region was reduced.

The results also showed that the observed changes in pressure distribution and force coefficients could be divided roughly into three regimes: $d/\delta_w>1$, $d/\delta_w<1$ and $d/\delta_1>1$, and $d/\delta_1<\sim1$. Different characteristic parameters behaved differently in these regimes.

For the aerodynamic force coefficients, it was found that gap width had a drastic impact when d/δ_1 was comparable to or less than one. In that case, a reduction in drag and an increase in lift coefficients were observed.

References

1. Clauser, F. H., (1954), "Turbulent boundary layers in adverse pressure gradients," *J. Aero. Sciences*, February, 1954, pp. 91-108.
2. Coles, D., (1956), "The law of the wake in the turbulent boundary layer," *J. Fluid Mech.*, Vol. 1, pp. 191-226.
3. Sakulyanontvittaya, T., Ngow, P., Prasartkarnkha, A., Chalokepunrat, S., Pimpin, A., and Bunyajitradulya, A., (1999), "The Design and Development of The FMRL 60x18 cm^2 Wide-Angle Screened-Diffuser Blower Tunnel Part III: The Settling Chamber, The Contraction, and The Wind Tunnel," Proceeding of the 13th National Mechanical Engineering Conference, 2-3 December 1999, Royal Cliff Beach Resort Hotel, South Pattaya, Cholburi.
4. White, F. M., (1994), Fluid Mechanics, Third Edition, McGraw Hill, New York.

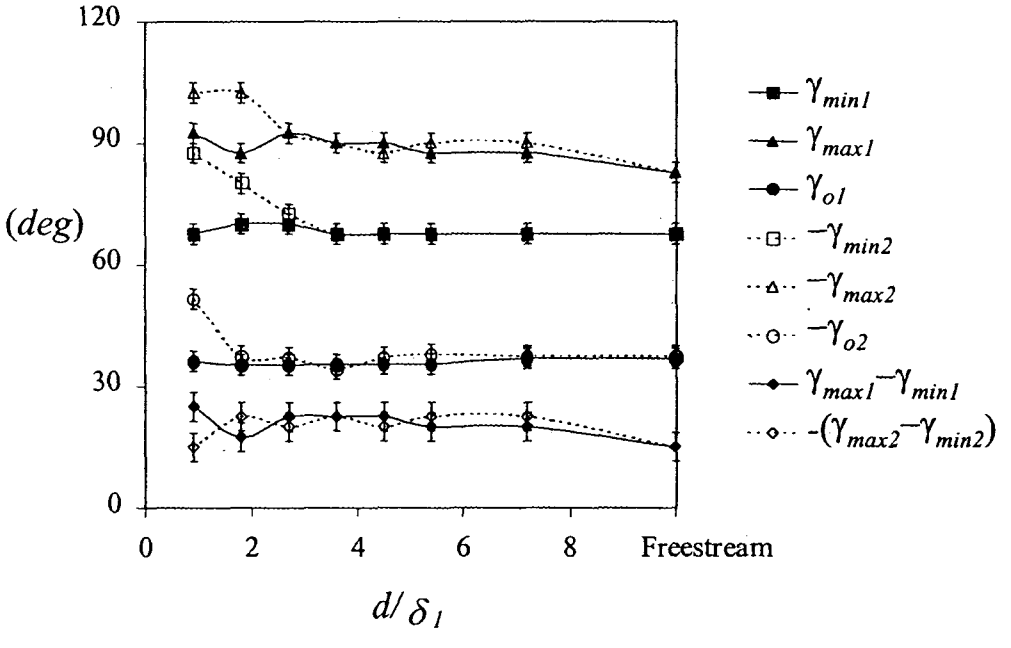

Fig. 9. Characteristic angles for the cylinder in subcritical flow with Re_D =1.6x10^4, δ_w / D =1, and δ_1 / D =0.26. Legends for the ordinates are on the right.

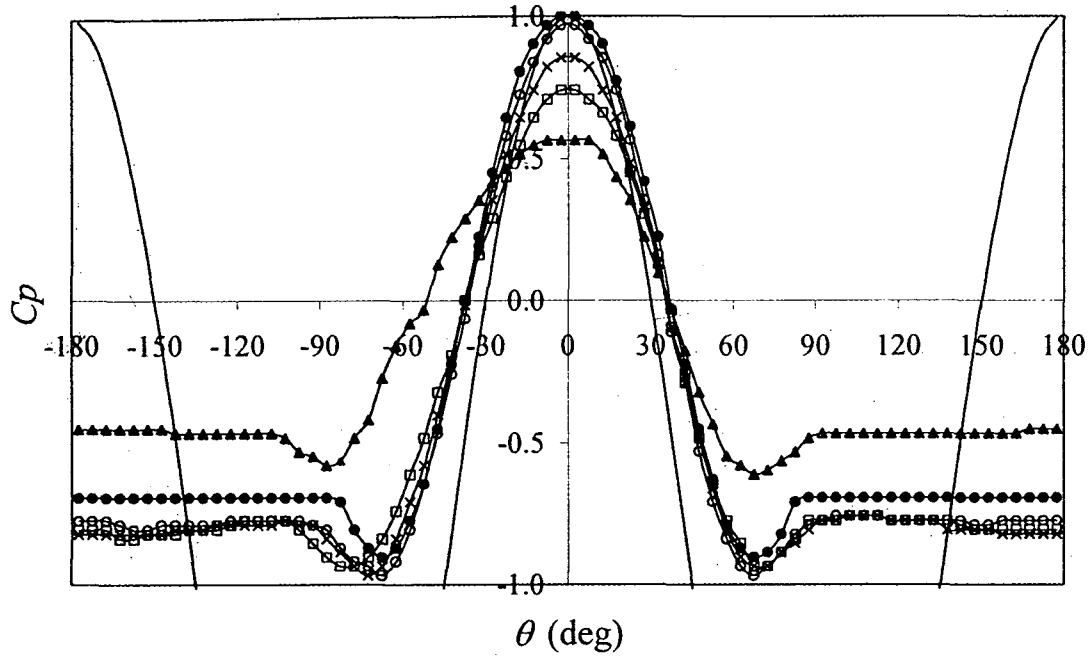

(a)

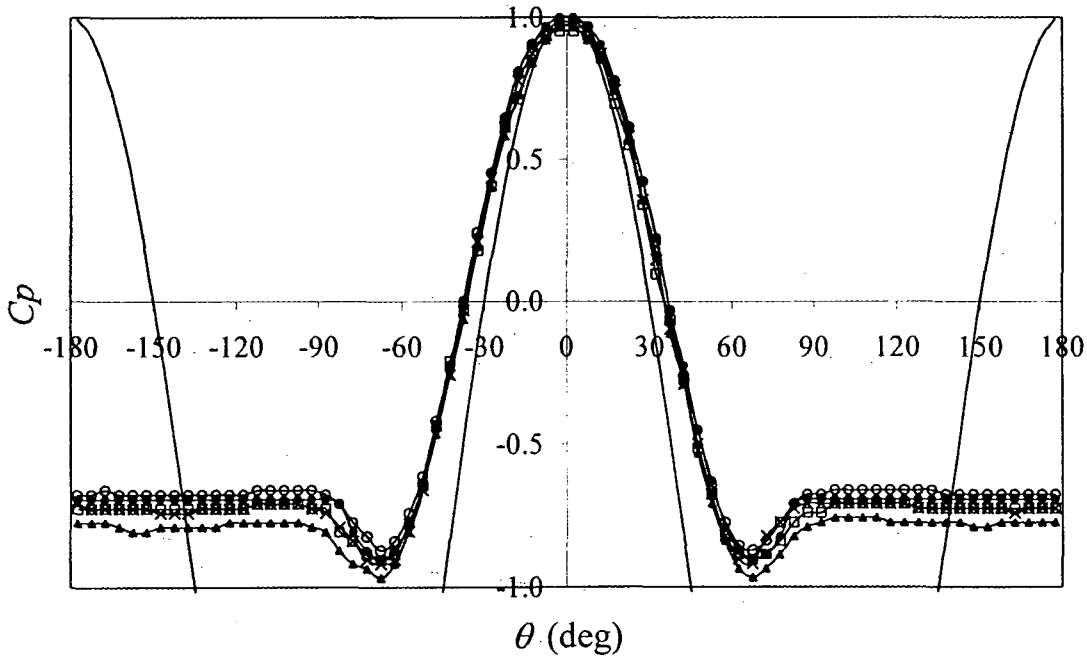

(b)

Fig. 5. Ground effect on static pressure distribution on the circumference of a cylinder in subcritical flow, $Re_D = 1.6 \times 10^4$, $\delta_w / D = 1$, $\delta_1 / D = 0.26$: (a) for cases $d/\delta_w < 1$: $d/\delta_1 = 0.9$, 1.8, and 2.7 (b) for cases $d/\delta_w > 1$: $d/\delta_1 = 4.5$, 5.4, and 7.2. Cases $d/\delta_1 = 3.6$ ($d/\delta_w = 0.94$) and ∞ are repeated in both figures for comparison.

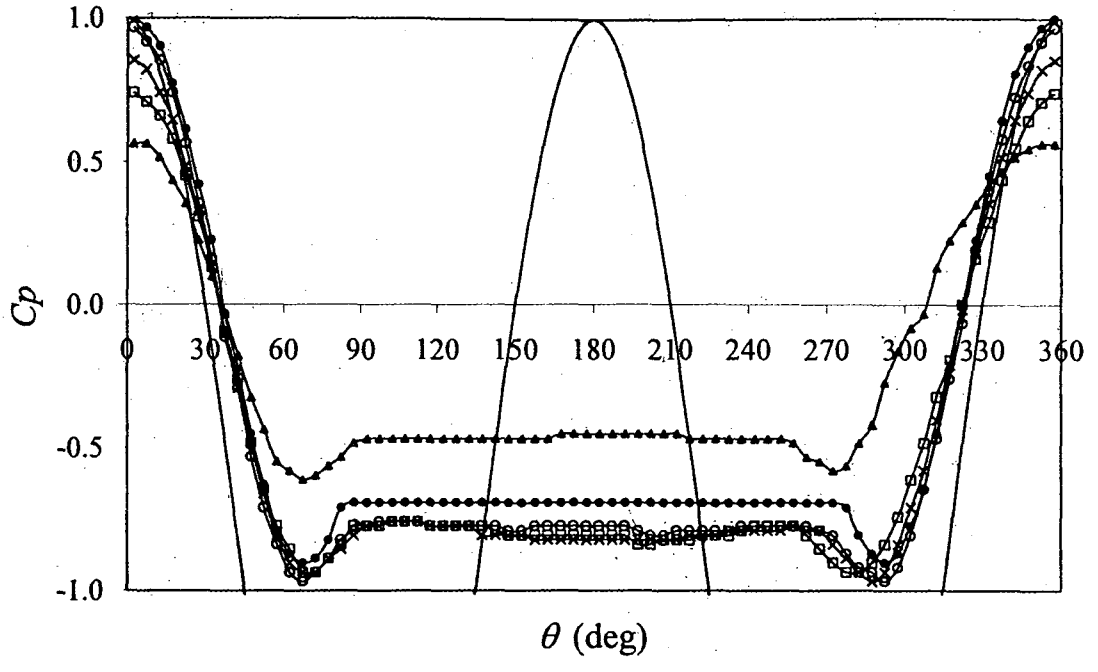

(a)

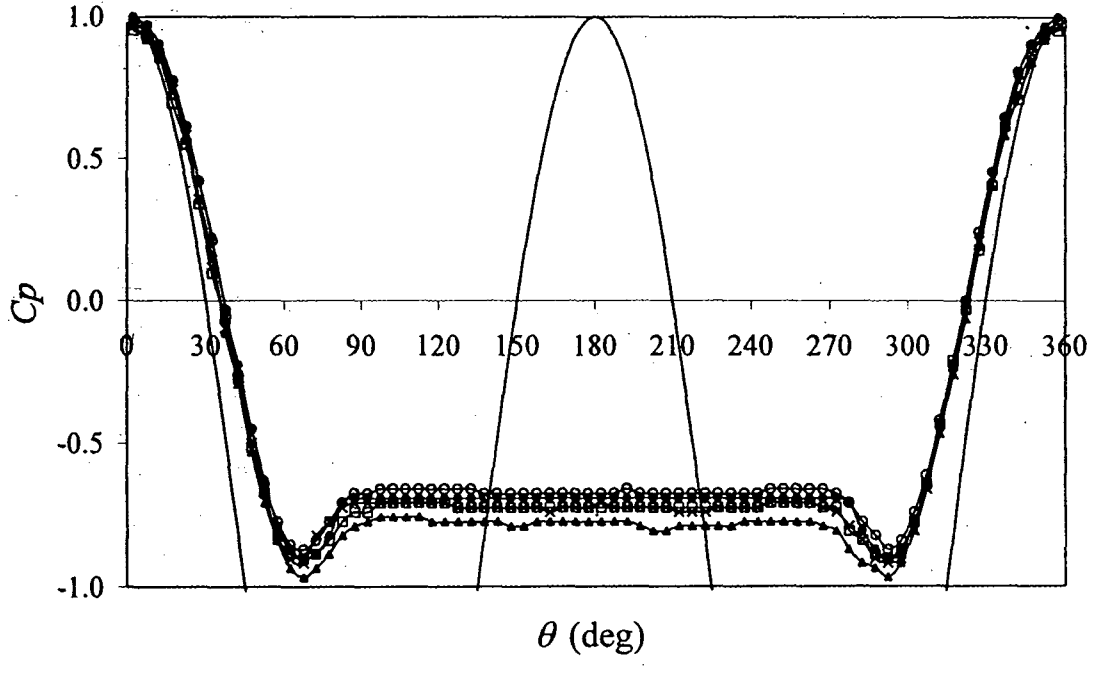

(b)

Fig. 10. A replot of Fig. 5 using different coordinates system ($0° < \theta < 360°$) illustrating the relative extent of the wake regions.

Table 1. Summary of the characteristics of ground effects on the cylinder in subcritical flow with $Re_D = 1.6 \times 10^4$, $\delta_w / D = 1$, and $\delta_1 / D = 0.26$. The number in parentheses indicates the estimate of experimental uncertainty.

	d/δ_1							
	0.9	1.8	2.7	3.6	4.5	5.4	7.2	∞
d/δ_w	0.22	0.46	0.7	0.94	1.18	1.42	1.9	∞
C_{pmax} (± 0.03)	0.57	0.74	0.86	0.97	0.95	0.97	0.98	1.0
C_{pmin1} (± 0.03)	-0.61	-0.94	-0.94	-0.97	-0.90	-0.92	-0.87	-0.90
C_{pmin2} (± 0.03)	-0.58	-0.94	-0.97	-0.97	-0.90	-0.92	-0.87	-0.90
C_{pw} (± 0.03)	-0.46	-0.80	-0.80	-0.78	-0.72	-0.72	-0.67	-0.69
C_{pw}-C_{pmin1} (± 0.04)	0.15	0.14	0.14	0.19	0.18	0.20	0.20	0.21
C_{pw}-C_{pmin2} (± 0.04)	0.12	0.14	0.17	0.19	0.18	0.20	0.20	0.21
γ_{min1} (± 2.5°)	68	70	70	68	68	68	68	68
$\gamma_{min2\ 1}$ (± 2.5°)	-89	-80	-73	-68	-68	-68	-68	-68
$\gamma_{max1\ 1}$ (± 2.5°)	93	88	93	90	90	88	88	83
$\gamma_{max2\ 1}$ (± 2.5°)	-103	-103	-93	-90	-88	-90	-90	-83
$\Delta\gamma_{min\ 1}$ (± 3.5°)	205	210	218	225	225	225	225	225
$\Delta\gamma_{max\ 1}$ (± 3.5°)	165	170	175	180	183	183	183	195
$\lvert\gamma_{max1}$-$\gamma_{min1}\rvert_1$ (± 3.5°)	25	18	23	23	23	20	20	15
$\lvert\gamma_{max2}$-$\gamma_{min2}\rvert$ (± 3.5°)	15	23	20	23	20	23	23	15
γ_{o1} (± 2.5°)	36	35	35	35	36	36	37	37
γ_{o2} (± 2.5°)	-52	-38	-37	-34	-37	-38	-38	-38
C_L (± 0.01)	0.11	0	0	0	0	0	0	0
C_D (± 0.01)	0.64	0.88	0.91	0.92	0.87	0.88	0.86	0.88
C_L/C_D (± 0.02)	0.17	0	0	0	0	0	0	0